Biogeosciences Discuss., 12, 5907–5940, 2015
www.biogeosciences-discuss.net/12/5907/2015/
doi:10.5194/bgd-12-5907-2015

Biogeosciences
Discussions
Open Access

Quantifying the influence of CO_2 seasonality on future ocean acidification

T. P. Sasse[1], B. I. McNeil[1], R. J. Matear[2], and A. Lenton[2]

[1]Climate Change Research Centre, Kensington Campus, University of New South Wales, Sydney, Australia
[2]CSIRO Oceans and Atmosphere National Research Flagship, Hobart, Australia

Received: 31 March 2015 – Accepted: 31 March 2015 – Published: 22 April 2015

Correspondence to: T. P. Sasse (t.sasse@unsw.edu.au)

Published by Copernicus Publications on behalf of the European Geosciences Union.

Abstract

Ocean acidification is a predictable consequence of rising atmospheric carbon dioxide (CO_2), and is highly likely to impact the entire marine ecosystem – from plankton at the base to fish at the top. Factors which are expected to be impacted include reproductive health, organism growth and species composition and distribution. Predicting when critical threshold values will be reached is crucial for projecting the future health of marine ecosystems and for marine resources planning and management. The impacts of ocean acidification will be first felt at the seasonal scale, however our understanding how seasonal variability will influence rates of future ocean acidification remains poorly constrained due to current model and data limitations. To address this issue, we first quantified the seasonal cycle of aragonite saturation state utilizing new data-based estimates of global ocean surface dissolved inorganic carbon and alkalinity. This seasonality was then combined with earth system model projections under different emissions scenarios (RCPs 2.6, 4.5 and 8.5) to provide new insights into future aragonite under-saturation onset. Under a high emissions scenario (RCP 8.5), our results suggest accounting for seasonality will bring forward the initial onset of month-long under-saturation by 17 years compared to annual-mean estimates, with differences extending up to 35 ± 17 years in the North Pacific due to strong regional seasonality. Our results also show large-scale under-saturation once atmospheric CO_2 reaches 486 ppm in the North Pacific and 511 ppm in the Southern Ocean independent of emission scenario. Our results suggest that accounting for seasonality is critical to projecting the future impacts of ocean acidification on the marine environment.

1 Introduction

The global ocean currently absorbs about 30 % of annual fossil-fuel CO_2 emissions (Le Quéré et al., 2012), and will likely sequester up to 80 % of all human-derived CO_2 emissions over the coming centuries (Archer et al., 1997). While this ecosystem service

BGD
12, 5907–5940, 2015

largely mediates the rate of climate change, the immediate impact of this additional CO_2 is a shift in the oceans chemical composition, resulting in lower pH and carbonate ion (CO_3^{2-}) concentrations – commonly referred to as ocean acidification (OA; Caldeira and Wickett, 2003).

Of great concern is the immediate impact OA is presenting to multiple marine organisms. This includes organisms that require an adequate supply of CO_3^{2-} to form and preserve their calcium carbonate ($CaCO_3$) shells and skeletons (e.g. corals, pteropods and coccolithophorids). Two key parameters for understanding how a change in CO_3^{2-} impacts marine calcifiers are the saturation states for aragonite (Ω_{Ar}; Eq. 1) and calcite (Ω_{Ca}; Eq. 2) – the two main $CaCO_3$ minerals formed by marine calcifiers.

$$\Omega_{Ar} = [Ca^{2+}][CO_3^{2-}]/K^*_{sp(Ar)} \quad (1)$$

$$\Omega_{Ca} = [Ca^{2+}][CO_3^{2-}]/K^*_{sp(Ca)} \quad (2)$$

Here, $[Ca^{2+}]$ and $[CO_3^{2-}]$ represent the concentrations of calcium and carbonate ions respectively, while $K^*_{sp(Ar)}$ and $K^*_{sp(Ca)}$ are the apparent stoichiometric solubility products for aragonite and calcite respectively. Laboratory and mesocosm experiments suggest production and dissolution of biogenic $CaCO_3$ are mainly controlled by seawater Ω levels (Aze et al., 2014; Fabry et al., 2008). These experiments further indicate significant decreases in calcification rates when test species are exposed to Ω levels below their natural range for periods of days to weeks (Chan and Connolly, 2013). Once seawater Ω levels fall below 1, referred to as under-saturation, seawater becomes corrosive to $CaCO_3$ and dissolution can occur. Although experimental studies show detrimental impacts at seawater Ω levels above 1 (e.g., Bednarsek et al., 2012; Fabry et al., 2008), under-saturation is widely regarded as a key threshold value (e.g., Hunt et al., 2008; Orr et al., 2005). Since aragonite is about 50 % more soluble than calcite, resulting in earlier under-saturation, we focus on future changes in Ω_{Ar}.

Several previous studies have used Earth System Models (ESM) to predict future annual-mean Ω_{Ar} levels under different CO_2 emission scenarios (Caldeira and Wickett,

BGD
12, 5907–5940, 2015

2003, 2005; Cao et al., 2007; Kleypas et al., 1999; Orr et al., 2005; Ricke et al., 2013). These annual-mean projections suggest under-saturation will occur in the Southern Ocean and high northern latitudes within the 21st century (e.g. Orr et al., 2005). However, strong natural seasonality in oceanic CO_2 within these regions has the potential to significantly alter the onset of future under-saturation, not captured by these approaches.

McNeil and Matear (2008) first demonstrated how strong CO_2 seasonality in the Southern Ocean brings forward the initial onset of month-long aragonite under-saturation conditions by ~ 30 years relative to annual-mean projections. More recent studies in Australia's Great Barrier Reef (Shaw et al., 2013), Californian coast (Gruber et al., 2012) and Arctic Ocean (Steinacher et al., 2009) further demonstrate the importance of accounting for natural CO_2 seasonality when evaluating future OA levels.

Despite significant efforts over recent years to establish a global carbon measurement network (e.g. the Global Ocean Acidification Observation Network; www.goa-on.org), such a large-scale initiative remains very limited, resulting in only a limited understanding of CO_2 seasonality throughout the global ocean (Monteiro et al., 2010). This represents a critical gap in our ability to understand and predict the influence of natural variability for the future onset and duration of critical OA levels.

It is important to note that ESM do provide some insights into regional CO_2 seasonality. However, it has been shown the current generation of ESM do not accurately capture the observation-based magnitude and/or phase of air–sea CO_2 fluxes in most ocean regions, including the Southern Ocean, North Pacific, Indian Ocean and North Subpolar Atlantic (Ishii et al., 2014; Lenton et al., 2013; Sarma et al., 2013; Schuster et al., 2009). Consequently, these models do not realistically characterize the seasonality of Ω_{Ar}.

Here, we use newly constrained data-based estimates of global ocean surface dissolved inorganic carbon (C_T) and alkalinity (A_T) to diagnose monthly Ω_{Ar} distributions for the nominal year of 2000. We then project our monthly observational baselines through to 2100 using decadal trends from an ensemble of Earth System climate mod-

BGD
12, 5907–5940, 2015

els (CMIP5) forced under different emissions scenarios (RCPs 2.6, 4.5 and 8.5). These results provide new insights into the influence of sea-surface seasonality on the likely onset times for future aragonite under-saturation in the global ocean.

The work presented here expands on the study of McNeil and Matear (2008) with several key improvements: (1) the new global CO_2 climatologies better reflect the latest observations and were derived using a more sophisticated method, (2) we explore the potential for CO_2 disequilibrium to evolve into the future by exploiting CMIP5 model projections, (3) we project our observational baseline using three different emission scenarios (RCP2.6, 4.5 and 8.5), (4) we apply the approach globally rather than the Southern Ocean alone.

2 Diagnosing monthly carbon system distributions

The oceans inorganic carbon system can be fully constrained by knowing any two parameters within its inorganic carbon constituents – partial pressure of CO_2 (pCO_2), dissolved inorganic carbon (C_T), total alkalinity (A_T) or pH (Dickson et al., 2007). Here we diagnose monthly Ω_{Ar} distributions using the newly constrained $1^\circ \times 1^\circ C_T$ and A_T monthly climatologies of Sasse et al. (2013a) in combination with the World Ocean Atlas 2013 (WOA13) temperature, salinity, and nutrient monthly surface distributions (Objectively analysed decadal averages; Garcia et al., 2014a, b; Locarnini et al., 2013; Zweng et al., 2013). Since the C_T climatologies of Sasse et al. (2013a) were predicted for the nominal year of 2000 (see Sasse et al., 2013a for details), the Ω_{Ar} values calculated here also represent the nominal year of 2000.

All calculations were conducted using the total pH scale and carbonic acid dissociation constants of Mehrbach et al. (1973) as refitted by Dickson and Millero (1987), K_{SO_4} dissociation constant of Dickson (1990a) and boric acid dissociation constant of Dickson (1990b). Calculations of Ω_{Ar} used the K_{sp} values of Mucci (1983) and [Ca]-salinity relationship of Riley and Tongudai (1967).

BGD
12, 5907–5940, 2015

To evaluate the realism of our global Ω_{Ar} predictions, we compare the network of in-situ Ω_{Ar} values to our corresponding $1^\circ \times 1^\circ$ predictions for the same month (Fig. 1). In-situ Ω_{Ar} values were calculated using measured A_T and C_T concentrations, where C_T values were first normalised to the year 2000 via observed Revelle factors and assuming constant equilibrium with the atmospheric CO_2 increase (see Sasse et al., 2013a for details). Our data-based approach is consistent with the general pattern of high Ω_{Ar} values in the tropics which decrease poleward. Our approach also captures well the strong Ω_{Ar} gradients at $\sim 40^\circ$ North and South and local Ω_{Ar} minimas in equatorial upwelling regions (see Fig. S1 in the Supplement for monthly Ω_{Ar} distributions). Statistical analysis finds the root mean square difference (RMSD) and correlation between the global in-situ values and our corresponding space/month $1^\circ \times 1^\circ$ predictions to be 0.17 and 0.98 respectively.

We further compare our zonal mean $1^\circ \times 1^\circ$ Ω_{Ar} predictions for summer and winter to the in-situ measurements to evaluate the ability of our approach to capture seasonal variability (Fig. 2). Our data-based reconstruction compares well to the general zonal pattern, showing a strong winter-time minimum in the higher latitudes. This winter-time signal is driven by the combination of cooling and strong persistent winds that ventilate deep-waters depleted in CO_3^{2-} (McNeil and Matear, 2008).

Our monthly data-based Ω_{Ar} distribution reconfirms that the contemporary ocean surface is supersaturated with respect to aragonite, showing 99.3 % of monthly ocean surface waters with Ω_{Ar} levels greater than 1 in the year 2000. The only region where month-long under-saturation was found is in the Arctic Ocean (see Fig. S2), which is consistent with previous data-based studies (e.g. Popova et al., 2014).

An independent data-based climatology for monthly ocean surface Ω_{Ar} was presented by Takahashi et al. (2014; hereinafter referred to as T14). In their approach, global Ω_{Ar} distributions were calculated for the nominal year of 2005 on a $4^\circ \times 5^\circ$ resolution using a combination of interpolated ocean-surface pCO_2 and predicted A_T values via a salinity and nitrate relationship. Estimates in the equatorial Pacific were however omitted due to strong inter-annual variability.

BGD
12, 5907–5940, 2015

Comparison between T14 and our global Ω_{Ar} values (projected to the year 2005; see Sect. 6) reveals a global correlation of 0.99, with mean Ω_{Ar} values of 2.68 and 2.72 respectively. This good agreement between two independent data-based approaches provides additional confidence in our estimated Ω_{Ar} values. Several key benefits in using our Ω_{Ar} baseline include: (1) better spatial resolution, (2) inclusion of the equatorial Pacific, (3) independent uncertainty estimates in our Ω_{Ar} predictions.

3 Quantifying uncertainties in our Ω_{Ar} predictions

The approach used here to diagnose surface Ω_{Ar} distributions includes both systematic and random sources of error. The main source of random error derives from uncertainties within the global C_T and A_T distributions, which have been estimated to be ±10.9 and ±9.2 $\mu mol\,kg^{-1}$ respectively (Sasse et al., 2013a). To quantify the corresponding uncertainty in our calculated Ω_{Ar} values, we applied an independent testing approach using 16 727 mixed-layer C_T and A_T independent predictions of Sasse et al. (2013a). In this approach, Ω_{Ar} values were calculated using both the in-situ C_T and A_T measurements and their corresponding independent predictions. Comparison between these values revealed a global uncertainty in our Ω_{Ar} predictions to be ±0.14 (Residual Standard Error (RSE); Fig. 3a).

To evaluate our approach for systematic errors, we analysed the global distribution of residual errors via the independent testing approach described above (Fig. 3b). We further partitioned the residuals by season to evaluate for any temporal bias (see Fig. S3). The global, winter and summer residual error distributions all followed a normal distribution with mean residual errors of 0.004, 0.007 and 0.001, respectively. This suggests no strong spatial or temporal biases exist in our approach.

Finally, it is important to acknowledge that uncertainties and biases in the WOA13 objectively analysed products will influence our data-derived Ω_{Ar} distributions. Since error estimates in the WAO13 products remain uncertain, this source of uncertainty cannot be accounted for at this time. However, if we assume errors in WOA13 are

BGD
12, 5907–5940, 2015

uncorrelated and much smaller than errors associated with the carbonate system, then they will not significantly contribute to uncertainty in our calculated Ω_{Ar} values.

4 How large is contemporary seasonal variability?

Seasonal amplitudes were calculated here as the difference between the maximum and minimum monthly Ω_{Ar} values in each $1^\circ \times 1^\circ$ grid cell (Fig. 4). From a global perspective, seasonality was found to be 0.48 ± 0.28 (1σ), while strong regional mixing/upwelling regimes and/or biological production results in large spatial differences. In the high Northern latitudes (45 to 70° N) and Southern subtropics (20 to 45° S) for example, seasonality was found to be strongest at 0.77 ± 0.25 and 0.46 ± 0.14 (1σ) respectively, while seasonality in the equatorial region (20° N to 20° S) was found to be weakest at 0.34 ± 0.21.

From an OA perspective, regions where seasonality is strongest will have the largest implications for future onset of critical Ω_{Ar} levels. In the tropics for example, where aragonite secreting corals are abundant (Tupper et al., 2011), the relatively weak seasonality will result in little difference between month-long and annual-mean onset for future Ω_{Ar} levels. In the higher latitudes however, where seasonality is largest, the implications for future Ω_{Ar} onset will be much more pronounced.

It must be noted that our seasonal predictions will underestimate some coastal regions where limited data exists. Along the coastal Antarctic continent for example, in-situ data has shown seasonal Ω_{Ar} variability of up to 1.75 (McNeil et al., 2010), which is not captured by our approach.

5 Is seasonality the dominant mode of Ω_{Ar} variability?

Variability in the open-ocean CO_2 system is the combination of seasonal and interannual variability (IAV), with diurnal variability only playing a significant role in coastal waters (Aze et al., 2014).

BGD
12, 5907–5940, 2015

To quantify the relative roles of seasonal and IAV in open-ocean waters, we analysed results from an ensemble of 6 ESM participating in the Coupled Model Intercomparison 5 project (CMIP5; Table 1). Each model was first re-gridded to a $1^\circ \times 1^\circ$ resolution via a binominal interpolation, and Ω_{Ar} values calculated via the standard CO_2 dissociation constants described in Sect. 2. To constrain the total magnitude of natural variability, we combined the seasonal and IAV signals within each $1^\circ \times 1^\circ$ grid cell (Fig. 5a). For IAV, we de-trended annual-mean values between 2006 and 2100 via a third order polynomial, and then calculated the SD in the de-trended data (i.e. 95.4 % of the year-to-year variance). For seasonality, we used the average seasonal magnitude (maximum minus minimum) between 2006 and 2016. The relative roles of variability were finally quantified by dividing the individual components by the total variability. We also multiplied these values by 100 to present the relative roles of seasonal variability and IAV as a percentage of the total natural variability (Fig. 5b and c).

This analysis revealed that seasonality is the dominant mode of variability throughout the global ocean, accounting for 74 ± 12 % (1σ) of total natural variability. From a regional perspective, seasonality is the dominant mode in the higher latitudes, accounting for 84 ± 5 % of total variability in the Southern Ocean (South of 30° S) and North Pacific (30 to 70° N). In the eastern equatorial Pacific however, IAV is the dominant mode of variability, representing up to 70 % of total variability (Fig. 5c). With the exception of the central equatorial Pacific, seasonality is the dominant mode of variable across the greater equatorial region (30° S to 30° N), accounting for 67 ± 12 % of the total natural variability within this region (Fig. 5b).

Comparison between our data-based Ω_{Ar} seasonal amplitudes (Fig. 4) and model-based total variability (Fig. 5a), reveals a consistent spatial pattern in regions where seasonality is the dominant mode (i.e. North Pacific, Southern Ocean and West North Atlantic). Despite this general agreement, we find that our data-based seasonal estimates are on average 1.3 times larger than the 2006–2016 model-based mean seasonal amplitudes in the North Atlantic, North Pacific and Southern Ocean (see Fig. S4).

BGD
12, 5907–5940, 2015

This suggests ESM under-predict the oceans seasonal CO_2 cycle and therefore its role in driving the total natural variability.

6 Projecting future Ω_{Ar} levels

Exchange of CO_2 between the ocean and atmosphere is driven by the air–sea gradient in pCO_2. Each year, approximately 70 petagrams of carbon is naturally exchanged at the air–sea interface in both directions (Sarmiento and Gruber, 2002). Comparison between ocean-surface and atmospheric pCO_2 reveals seasonality in the ocean is the dominant driver of this large natural CO_2 flux (Sasse et al., 2013b; Takahashi et al., 2009), which in turn is driven by biological and physical-solubility processes (Sarmiento and Gruber, 2006) – referred to here as the natural cycling of carbon.

If the natural cycling of carbon remained in steady-state throughout the last two centuries, the rate of increase in ocean surface pCO_2 would have roughly tracked the atmospheric CO_2 growth rate. Although this was likely adequate for most of the 20th century, recent studies have identified shifts in the oceans natural cycling of carbon due to climate related alterations. For example, decadal-scale trends in ocean surface temperature (Levitus et al., 2005; Lyman et al., 2010) and salinity (Durack and Wijffels, 2010) are influencing both the solubility of CO_2 and ocean circulation pathways, while shifting wind patterns are impacting circulation and seasonal mixing processes, resulting in either enhanced or diminished ventilation of deep waters enriched with C_T and nutrients (e.g. Le Quéré et al., 2007; Lenton et al., 2009).

Added to this climate-mediated change in oceanic CO_2 uptake, the air–sea exchange of CO_2 is a slow process (approximately 1 year equilibration time), where physical and biological processes can cause the ocean to deviate from atmospheric CO_2. This creates a difference between the atmosphere and ocean surface pCO_2 (disequilibrium). Further, as atmospheric CO_2 increases, ocean processes can cause the ocean to lag the atmospheric increase and the disequilibrium term to increase with time. For example, in the polar regions, short residence times of surface waters and the ventilation

BGD
12, 5907–5940, 2015

of old CO_2-rich deep waters creates an increasing CO_2 disequilibrium, resulting in a growing difference between atmospheric and surface ocean CO_2 over time.

To account for the effects of future climate change and increasing CO_2 disequilibrium, we projected our data-based CO_2 climatologies using results from an ensemble of 6 ESM (Table 1). In this approach, decadal trends in C_T, A_T, temperature and salinity were combined with our monthly data-based C_T and A_T and WOA13 temperature and salinity products. Monthly Ω_{Ar} values were then calculated using the standard CO_2 dissociation constants presented in Sect. 2.

We projected our CO_2 base-lines using ESM results forced under several different Representative Concentration Pathways (RCP8.5, 4.5 and 2.6). Here, RCP8.5 is a *business-as-usual* scenario with little mitigation and peak CO_2 concentrations at 935 parts per million (ppm) in the year 2100; RCP4.5 is a scenario where emissions peak in mid-century and are then slowly reduced, resulting in a peak CO_2 concentration of 538 ppm by 2100; finally, RCP2.6 is a *best-case* scenario were emissions are dramatically reduced in the near future to the point where more CO_2 is absorbed by the ocean and terrestrial biosphere than emitted by human activities (Meinshausen et al., 2011).

It should be emphasised that the observation-based CO_2 climatologies of Sasse et al. (2013a) have been shown to accurately reconstruct the global pattern of present-day ocean surface CO_2 variability. However, for this study we assume constant seasonality from our baseline CO_2 climatologies throughout the 21st century. Although this assumption is likely adequate for short temporal projections (< 10 years), a recent evaluation of 10 ESM suggests large changes in mixing, biological production and CO_2 solubility will occur within the 21st century (Bopp et al., 2013). By projecting our baseline climatologies using decadal trends from ESM we implicitly capture the decadal response to these changes, however, any potential shift in the phase and magnitude of CO_2 seasonality are not explored in our approach.

Given the limitations in the current generation of ESM in capturing seasonality in air–sea CO_2 flux and/or ocean surface pCO_2 in many important regions (Ishii et al., 2014; Lenton et al., 2013; Sarma et al., 2013; Schuster et al., 2009), their ability to

BGD
12, 5907–5940, 2015

realistically project future changes in CO_2 seasonality is questionable. We therefore do not account for any change in CO_2 seasonality in the current study. Once models evolve to a point where seasonality of the carbon system is well-represented, potential future changes to seasonality will need to be explored in future studies.

7 Quantifying the onset of aragonite under-saturation

When strong natural carbon seasonality is combined with a long-term trend, the onset and exposure times of biological thresholds are influenced. To illustrate this point, we present Ω_{Ar} projections under the *business-as-usual* scenario (RCP8.5) at two unique sites in the North Atlantic and Southern Ocean (Fig. 6). At the North Atlantic site, strong seasonality was found to bring forward the initial onset (time a in Fig. 6a) of aragonite under-saturation by 27 years relative to the annual-mean (time b; Fig. 6a), while weaker variability at the Southern Ocean site brings forward under-saturation by 8 years (Fig. 6b). It's important to emphasize that monthly under-saturation conditions starts at time a, and then eventually extends to be permanent over all months (time c). As much as seasonality brings forward the initial onset of under-saturation, it also delays the permanent onset (Fig. 6). At the Southern Ocean site for example, seasonality delays the permanent onset by ~ 15 years. In the context of ocean acidification impacts, monthly exposure times are important, since laboratory experiments show that even short exposure times (i.e. days to weeks) can result in significant implications to the health and well-being of the test species (Chan and Connolly, 2013).

Note that our reconstructed seasonal amplitudes were initially constant, however as ocean carbon chemistry changed with additional CO_2 input (i.e. changes in the Revelle factor), the amplitudes of the calculated Ω_{Ar} reduced.

BGD
12, 5907–5940, 2015

7.1 Future Ω_{Ar} levels under RCP8.5

Under the *business-as-usual* scenario (RCP8.5), our results show annual-mean aragonite under-saturation will occur by 2086 ± 9 (1σ) in the North Pacific and North Atlantic, 2074 ± 12 in the Southern Ocean, while tropical and temperate regions (~ 40° S to ~ 40° N) will remain super-saturated beyond centuries end (Fig. 7a). When seasonality is considered, the initial month-long onset precedes annual-mean estimates by a global average of 17 years under the RCP8.5 scenario (70° N to 70° S; Fig. 7b and c). In the North Pacific and North Atlantic, where seasonality is strongest, month-long under-saturation is brought forward by 38 ± 18 and 20 ± 7 years respectively (Fig. 7c).

In the Southern Ocean (South of 60° S), our results show month-long aragonite under-saturation will first occur as early as 2030, or when atmospheric CO_2 concentrations reach ~ 450 ppm. While this is consistent with projections by McNeil and Matear (2008) under the IPCC IS92a scenario, our results show seasonality will delay the onset of annual-mean under-saturation by 14 ± 6 years, which is half the delay time found by McNeil and Matear (i.e. 30 years; 2008). This difference likely reflects the faster rate of change in atmospheric CO_2 under RCP8.5 compared to IPCC IS92a, while differences in seasonality found by the two approaches is likely a secondary factor.

Early aragonite under-saturation is of particular concern for the many important calcifying organisms that inhabit the higher latitudes. Pteropods for example, are a zooplankton species that forms aragonite shells to provide ballast for vertical migration in search of food and breeding. In the Southern Ocean, pteropods have been found to represent up to 30 % of total zooplankton (Hunt et al., 2008), and are themselves important prey for larger zooplankton, as well as many fish and bird species (Hunt et al., 2008; Karnovsky et al., 2008). From a biogeochemical perspective, pteropods account for at least 12 % of the global $CaCO_3$ flux into the ocean interior (Berner and Honjo, 1981). When pteropods sink to depths at which $\Omega_{Ar} = 1$, known as the saturation horizon or lysocline, field studies show significant dissolution occurs (Hunt et al., 2008). As more anthropogenic CO_2 enters the ocean system, the aragonite saturation

BGD
12, 5907–5940, 2015

horizon will approach the upper ocean until the surface waters become permanently under-saturated. Before this occurs however, seasonal variability will expose calcifying organisms to month-long under-saturation conditions decade(s) before the annual mean value becomes under-saturated.

7.2 Future Ω_{Ar} levels under RCP 4.5 and 2.6

In the previous section we presented results under the RCP8.5 scenario. We now explore how lower emission scenarios influence future onset of aragonite under-saturation. We consider our Ω_{Ar} projections under RCP4.5, 2.6 and their behaviour relative to RCP8.5 (Table 2 and Fig. 8). In the North Pacific, we find month-long aragonite under-saturation occurs by the year 2052 ± 27 and 2037 ± 18 under RCP4.5 and 8.5, respectively. Despite this difference in onset year, atmospheric CO_2 concentrations at time of onset are consistent at 481 ± 54 ppm and 491 ± 69 for RCP4.5 and 8.5 respectively, with a correlation co-efficient of 0.82 (Table 2). As expected, this suggests under-saturation onset is highly dependent on the atmospheric CO_2 concentration, where we find large scale under-saturation in the North Pacific once atmospheric CO_2 reaches 486 ppm (mean of RCP4.5 and 8.5). Similarly, our results suggest wide spread aragonite under-saturation will occur when atmospheric CO_2 reaches concentrations of 506 ppm in the North Atlantic and 511 ppm in the Southern Ocean.

To further probe the influence of a lower emission scenario on future OA onset, we compare the time difference between month-long and annual-mean aragonite under-saturation onset under RCP8.5 and RCP4.5 at 468 $1^\circ \times 1^\circ$ grid cell locations in Southern Ocean (Figs. 8a and 7b). Here we find the average onset for month-long under-saturation occurs by the year 2048 under RCP8.5, and 2073 under RCP4.5. Despite the lower emission scenario delaying the initial onset, we find that the time difference between month-long and annual mean onset is 18 years longer under RCP4.5 compared to RCP8.5 (i.e. 14 years under RCP8.5 and 32 years under RCP4.5). This longer time delay under RCP4.5 emphasizes that seasonality becomes even more important when projecting future OA levels under a slower emissions scenarios.

BGD
12, 5907–5940, 2015

8 How does seasonality influence the geographical extent of aragonite under-saturation?

Accounting for seasonality also presents significant implications for the spatial pattern of aragonite under-saturation by the end of the 21st century. Here we refer to regions where seasonality induces at least month-long under-saturation conditions while annual-mean Ω_{Ar} projections remain super-saturated throughout the 21st century. By the year 2100, the latitudinal extent of ocean surface exposed to at least month-long aragonite under-saturation will have increased by $\sim 3.5^{\circ}$ relative to the extent of annual-mean estimates under the RCP8.5 scenario (Fig. 9). This extension translates to an additional $\sim 25 \times 10^{6}$ km^{2} of ocean surface (or 7.2 % of total open-ocean area) exposed to at least month-long aragonite under-saturation by 2100 under the *business-as-usual* scenario (RCP8.5). This expansion of corrosive aragonite conditions is likely to impact marine calcifiers living within these regions much earlier than anticipated. Pteropods for example, represent up to 30 % of total zooplankton species around the Prince Edward Islands (PEI; Fig. 9; Hunt et al., 2008), if these stocks deplete under future OA levels, the many other animals that rely on pteropods as a source of food will also be detrimentally impacted.

9 Conclusions

Ocean acidification is a global issue which is likely to impact the entire marine ecosystem – from plankton at the base to fish at the top. Of particular concern is the decreasing concentration of CO_3^{2-} ions, which lowers the saturation states of $CaCO_3$ minerals (Ω_{Ar}) and results in detrimental seawater conditions for marine calcifiers (e.g. pteropods and corals; Aze et al., 2014; Fabry et al., 2008). Predicting when critical Ω_{Ar} threshold values will be reached is crucial for projecting the future health of marine ecosystems and for marine resources planning and management. The impacts of ocean acidification will be first felt at the seasonal scale, however our present constraint

BGD
12, 5907–5940, 2015

on Ω_{Ar} seasonality is poor due to current model and data limitations. This represents a critical gap in our ability to accurately diagnose the influence of seasonality on the future onset and duration of critical Ω_{Ar} levels.

To overcome this issue, we first exploited new monthly global C_T and A_T climatologies to diagnose monthly Ω_{Ar} distributions for the nominal year of 2000. We then applied an independent testing approach which revealed global uncertainties in our Ω_{Ar} predictions to be ±0.14, with no strong global or seasonal biases. Finally, we combined our observational baselines with decadal trends from an ensemble of ESM under different emissions scenarios (RCPs 2.6, 4.5 and 8.5) to project our monthly Ω_{Ar} distributions through to 2100. These results have provided new insights into the role of seasonality in setting future aragonite values and time of under-saturation onset in the global ocean.

The influence of seasonality was evaluated by comparing the difference in future month-long and annual-mean Ω_{Ar} under-saturation onset. Our results suggest seasonality brings forward the initial onset of month-long under-saturation by 17 years compared to annual mean estimates under RCP8.5, with differences extending up to 35 ± 17 years in the North Pacific due to strong regional seasonality.

Our results also show large-scale under-saturation once atmospheric CO_2 reaches 486 ppm in the North Pacific, 506 ppm in the North Atlantic and 511 ppm in the Southern Ocean, independent of emission scenario. It's important to note that seasonality in these regions was also found to be the dominate mode of variability, accounting for 84 ± 5 % of total model-based variability in the Southern Ocean (South of 30° S) and North Pacific (30 to 70° N). This suggests IAV will not significantly alter onset times found in this study.

Under lower emission scenarios, the average time difference between month-long and annual-mean aragonite under-saturation onset increased from 14 years under RCP8.5 to 32 years under RCP4.5 in the Southern Ocean. This larger time difference under a lower emissions scenario emphasizes the importance of accounting for seasonality when projecting future OA levels under a slower emissions scenario.

BGD
12, 5907–5940, 2015

Seasonality also influences the spatial pattern of future Ω_{Ar} under-saturation, expanding the latitudinal extent by a global average of 3.5° (or 25×10^6 km^2) compared to annual-mean projections under RCP8.5. From a biogeochemical perspective, this is particularly concerning given that the region of expansion (~ 40 to 50° South and North) is a known to be a hot spot for $CaCO_3$ export (Sarmiento and Gruber, 2006).

Finally, the implication of our results are not limited to the higher latitudes, strong Ω_{Ar} seasonality in some subtropical regions (30° S–30° N; see Fig. 4) will likely bring forward the onset of lower Ω_{Ar} waters by similar temporal periods. Since these regions are rich with sensitive calcifying coral reef ecosystems, considering the influence of seasonality is important when estimating future OA levels in these regions.

The Supplement related to this article is available online at doi:10.5194/bgd-12-5907-2015-supplement.

References

Archer, D., Kheshgi, H., Maier, and Reimer, E.: Multiple timescales for neutralization of fossil fuel CO_2, Geophys. Res. Lett., 24, 405–408, doi:10.1029/97gl00168, 1997.

Aumont, O. and Bopp, L.: Globalizing results from ocean in situ iron fertilization studies, Global Biogeochem. Cy., 20, GB2017, doi:10.1029/2005gb002591, 2006.

Aze, T., Barry, J., Bellerby, R., Brander, L., Byrne, M., Dupont, S., Gattuso, J.-P., Gibbs, S., Hansson, L., Hattam, C., Hauton, C., Havenhand, J., Fossa, J. H., Kavanagh, C., Kurihara, H., Matear, R., Mark, F., Melzner, F., Munday, P., Niehoff, B., Pearson, P., Rehdanz, K., Tambutte, S., Turley, C., Venn, A., Warnau, M., and Young, J.: An Updated Synthesis of the Impacts of Ocean Acidification on Marine Biodiversity, 1st edn., Technical Series No. 75, edited by: Hennige, S., Roberts, J. M., and Williamson, P., Montreal, 99 pp., Secretariat of the Convention on Biological Diversity, 2014.

Bednarsek, N., Tarling, G. A., Bakker, D. C. E., Fielding, S., Jones, E. M., Venables, H. J., Ward, P., Kuzirian, A., Leze, B., Feely, R. A., and Murphy, E. J.: Extensive dissolution of live pteropods in the Southern Ocean, Nat. Geosci., 5, 881–885, doi:10.1038/ngeo1635, 2012.

BGD
12, 5907–5940, 2015

Berner, R. A. and Honjo, S.: Pelagic sedimentation of aragonite: its geochemical significance, Science, 211, 940–942, doi:10.1126/science.211.4485.940, 1981.

Bopp, L., Resplandy, L., Orr, J. C., Doney, S. C., Dunne, J. P., Gehlen, M., Halloran, P., Heinze, C., Ilyina, T., Séférian, R., Tjiputra, J., and Vichi, M.: Multiple stressors of ocean ecosystems in the 21st century: projections with CMIP5 models, Biogeosciences, 10, 6225–6245, doi:10.5194/bg-10-6225-2013, 2013.

Caldeira, K. and Wickett, M. E.: Oceanography: anthropogenic carbon and ocean pH, Nature, 425, 365, doi:10.1038/425365a, 2003.

Caldeira, K. and Wickett, M. E.: Ocean model predictions of chemistry changes from carbon dioxide emissions to the atmosphere and ocean, J. Geophys. Res.-Oceans, 110, C09S04, doi:10.1029/2004JC002671, 2005.

Cao, L., Caldeira, K., and Jain, A. K.: Effects of carbon dioxide and climate change on ocean acidification and carbonate mineral saturation, Geophys. Res. Lett., 34, L05607, doi:10.1029/2006gl028605, 2007.

Chan, N. C. S. and Connolly, S. R.: Sensitivity of coral calcification to ocean acidification: a meta-analysis, Glob. Change Biol., 19, 282–290, doi:10.1111/gcb.12011, 2013.

Dickson, A. G.: Standard potential of the reaction: $AgCl(s) + 1/2H_2(g) = Ag(s) + HCl(aq)$, and and the standard acidity constant of the ion HSO_4^- in synthetic sea water from 273.15 to 318.15 K, J. Chem. Thermodyn., 22, 113–127, doi:10.1016/0021-9614(90)90074-Z, 1990a.

Dickson, A. G.: Thermodynamics of the dissociation of boric acid in synthetic seawater from 273.15 to 318.15 K, Deep-Sea Res. Pt. I, 37, 755–766, doi:10.1016/0198-0149(90)90004-F, 1990b.

Dickson, A. G. and Millero, F. J.: A comparison of the equilibrium constants for the dissociation of carbonic acid in seawater media, Deep-Sea Res. Pt. I, 34, 1733–1743, doi:10.1016/0198-0149(87)90021-5, 1987.

Dickson, A. G., Sabine, C. L., and Christian, J. R. (Eds.): Guide to Best Practices for Ocean CO_2 Measurements, PICES Special Publication 3, 191 pp., 2007.

Dunne, J. P., John, J. G., Shevliakova, E., Stouffer, R. J., Krasting, J. P., Malyshev, S. L., Milly, P. C. D., Sentman, L. T., Adcroft, A. J., Cooke, W., Dunne, K. A., Griffies, S. M., Hallberg, R. W., Harrison, M. J., Levy, H., Wittenberg, A. T., Phillips, P. J., and Zadeh, N.: GFDL's ESM2 global coupled climate–carbon earth system models. Part II: Carbon system formulation and baseline simulation characteristics, J. Climate, 26, 2247–2267, doi:10.1175/JCLI-D-12-00150.1, 2013.

BGD
12, 5907–5940, 2015

Durack, P. J. and Wijffels, S. E.: Fifty-year trends in global ocean salinities and their relationship to broad-scale warming, J. Climate, 23, 4342–4362, doi:10.1175/2010jcli3377.1, 2010.

Fabry, V. J., Seibel, B. A., Feely, R. A., and Orr, J. C.: Impacts of ocean acidification on marine fauna and ecosystem processes, ICES J. Mar. Sci., 65, 414–432, doi:10.1093/icesjms/fsn048, 2008.

Garcia, H. E., Locarnini, R. A., Boyer, T. P., Antonov, J. I., Baranova, O. K., Zweng, M. M., Reagan, J. R., and Johnson, D. R.: World Ocean Atlas 2013, Volume 3: Dissolved Oxygen, Apparent Oxygen Utilization, and Oxygen Saturation, edited by: Levitus, S. and Mishonov, A., NOAA Atlas NESDIS 75, 27 pp., Maryland, 2014a.

Garcia, H. E., Locarnini, R. A., Boyer, T. P., Antonov, J. I., Baranova, O. K., Zweng, M. M., Reagan, J. R., and Johnson, D. R.: World Ocean Atlas 2013, Volume 4: Dissolved Inorganic Nutrients (Phosphate, Nitrate, Silicate), edited by: Levitus, S. and Mishonov, A., NOAA Atlas NESDIS 76, 25, 25 pp., Maryland, 2014b

Gruber, N., Hauri, C., Lachkar, Z., Loher, D., Frölicher, T. L., and Plattner, G.-K.: Rapid progression of ocean acidification in the California current system, Science, 337, 220–223, doi:10.1126/science.1216773, 2012.

Hunt, B. P. V., Pakhomov, E. A., Hosie, G. W., Siegel, V., Ward, P., and Bernard, K.: Pteropods in Southern Ocean ecosystems, Prog. Oceanogr., 78, 193–221, doi:10.1016/j.pocean.2008.06.001, 2008.

Ilyina, T., Six, K. D., Segschneider, J., Maier-Reimer, E., Li, H., and Núñez-Riboni, I.: Global ocean biogeochemistry model HAMOCC: model architecture and performance as component of the MPI-Earth system model in different CMIP5 experimental realizations, Journal of Advances in Modeling Earth Systems, 5, 287–315, doi:10.1029/2012MS000178, 2013.

Ishii, M., Feely, R. A., Rodgers, K. B., Park, G.-H., Wanninkhof, R., Sasano, D., Sugimoto, H., Cosca, C. E., Nakaoka, S., Telszewski, M., Nojiri, Y., Mikaloff Fletcher, S. E., Niwa, Y., Patra, P. K., Valsala, V., Nakano, H., Lima, I., Doney, S. C., Buitenhuis, E. T., Aumont, O., Dunne, J. P., Lenton, A., and Takahashi, T.: Air–sea CO_2 flux in the Pacific Ocean for the period 1990–2009, Biogeosciences, 11, 709–734, doi:10.5194/bg-11-709-2014, 2014.

Karnovsky, N. J., Hobson, K. A., Iverson, S., and Hunt, G. L. J.: Seasonal changes in diets of seabirds in the North Water Polynya: a multiple-indicator approach, Mar. Ecol.-Prog. Ser., 357, 291–299, doi:10.3354/meps07295, 2008.

BGD
12, 5907–5940, 2015

Kleypas, J. A., Buddemeier, R. W., Archer, D., Gattuso, J.-P., Langdon, C., and Opdyke, B. N.: Geochemical consequences of increased atmospheric carbon dioxide on coral reefs, Science, 284, 118–120, doi:10.1126/science.284.5411.118, 1999.

Le Quéré, C., Rödenbeck, C., Buitenhuis, E. T., Conway, T. J., Langenfelds, R., Gomez, A., Labuschagne, C., Ramonet, M., Nakazawa, T., Metzl, N., Gillett, N., and Heimann, M.: Saturation of the Southern Ocean CO_2 sink due to recent climate change, Science, 316, 1735–1738, doi:10.1126/science.1136188, 2007.

Le Quéré, C., Andres, R. J., Boden, T., Conway, T., Houghton, R. A., House, J. I., Marland, G., Peters, G. P., van der Werf, G. R., Ahlström, A., Andrew, R. M., Bopp, L., Canadell, J. G., Ciais, P., Doney, S. C., Enright, C., Friedlingstein, P., Huntingford, C., Jain, A. K., Jourdain, C., Kato, E., Keeling, R. F., Klein Goldewijk, K., Levis, S., Levy, P., Lomas, M., Poulter, B., Raupach, M. R., Schwinger, J., Sitch, S., Stocker, B. D., Viovy, N., Zaehle, S., and Zeng, N.: The global carbon budget 1959–2011, Earth Syst. Sci. Data, 5, 165–185, doi:10.5194/essd-5-165-2013, 2013.

Lenton, A., Codron, F., Bopp, L., Metzl, N., Cadule, P., Tagliabue, A., and Le Sommer, J.: Stratospheric ozone depletion reduces ocean carbon uptake and enhances ocean acidification, Geophys. Res. Lett., 36, L12606, doi:10.1029/2009gl038227, 2009.

Lenton, A., Tilbrook, B., Law, R. M., Bakker, D., Doney, S. C., Gruber, N., Ishii, M., Hoppema, M., Lovenduski, N. S., Matear, R. J., McNeil, B. I., Metzl, N., Mikaloff Fletcher, S. E., Monteiro, P. M. S., Rödenbeck, C., Sweeney, C., and Takahashi, T.: Sea–air CO_2 fluxes in the Southern Ocean for the period 1990–2009, Biogeosciences, 10, 4037–4054, doi:10.5194/bg-10-4037-2013, 2013.

Levitus, S., Antonov, J., and Boyer, T.: Warming of the world ocean, 1955–2003, Geophys. Res. Lett., 32, L02604, doi:10.1029/2004gl021592, 2005.

Locarnini, R. A., Mishonov, A. V., Antonov, J. I., Boyer, T. P., Garcia, H. E., Baranova, O. K., Zweng, M. M., Paver, C. R., Reagan, J. R., Johnson, D. R., Hamilton, M., and Seidov, D.: World Ocean Atlas 2013, Volume 1: Temperature, edited by: Levitus, S. and Mishonov, A., NOAA Atlas NESDIS 73, 40 pp., Maryland, 2013.

Lyman, J. M., Good, S. A., Gouretski, V. V., Ishii, M., Johnson, G. C., Palmer, M. D., Smith, D. M., and Willis, J. K.: Robust warming of the global upper ocean, Nature, 465, 334–337, doi:10.1038/nature09043, 2010.

BGD
12, 5907–5940, 2015

McNeil, B. I. and Matear, R. J.: Southern Ocean acidification: a tipping point at 450-ppm atmospheric CO_2, P. Natl. Acad. Sci. USA, 105, 18860–18864, doi:10.1073/pnas.0806318105, 2008.

McNeil, B. I., Tagliabue, A., and Sweeney, C.: A multi-decadal delay in the onset of corrosive "acidified" waters in the Ross Sea of Antarctica due to strong air–sea CO_2 disequilibrium, Geophys. Res. Lett., 37, L19607, doi:10.1029/2010gl044597, 2010.

Mehrbach, C., Culberson, C. H., Hawley, J. E., and Pytkowicz, R. M.: Measurement of the apparent dissociation constants of carbonic acid in seawater at atmospheric pressure, Limnol. Oceanogr., 18, 897–907, 1973.

Meinshausen, M., Smith, S. J., Calvin, K., Daniel, J. S., Kainuma, M. L. T., Lamarque, J. F., Matsumoto, K., Montzka, S. A., Raper, S. C. B., Riahi, K., Thomson, A., Velders, G. J. M., and Vuuren, D. P. P.: The RCP greenhouse gas concentrations and their extensions from 1765 to 2300, Climatic Change, 109, 213–241, doi:10.1007/s10584-011-0156-z, 2011.

Monteiro, P., Schuster, U., Hood, M., Lenton, A., Metzl, N., Olsen, A., Rogers, K., Sabine, C., Takahashi, T., Tilbrook, B., Yoder, J., Wanninkhof, R., and Watson, A. J.: A Global Sea Surface Carbon Observing System: Assessment of Changing Sea Surface CO_2 and Air–Sea CO_2 Fluxes, Proceedings of OceanObs'09: Sustained Ocean Observations and Information for Society, Vol. 2, Venice, Italy, 21–25 September 2009, 64, 2010.

Mucci, A.: The solubility of calcite and aragonite in seawater at various salinities, temperatures, and one atmosphere total pressure, Am. J. Sci., 283, 780–799, doi:10.2475/ajs.283.7.780, 1983.

Orr, J. C., Fabry, V. J., Aumont, O., Bopp, L., Doney, S. C., Feely, R. A., Gnanadesikan, A., Gruber, N., Ishida, A., Joos, F., Key, R. M., Lindsay, K., Maier-Reimer, E., Matear, R., Monfray, P., Mouchet, A., Najjar, R. G., Plattner, G.-K., Rodgers, K. B., Sabine, C. L., Sarmiento, J. L., Schlitzer, R., Slater, R. D., Totterdell, I. J., Weirig, M.-F., Yamanaka, Y., and Yool, A.: Anthropogenic ocean acidification over the twenty-first century and its impact on calcifying organisms, Nature, 437, 681–686, doi:10.1038/nature04095, 2005.

Palmer, J. R. and Totterdell, I. J.: Production and export in a global ocean ecosystem model, Deep-Sea Res. Pt. I, 48, 1169–1198, doi:10.1016/S0967-0637(00)00080-7, 2001.

Popova, E. E., Yool, A., Aksenov, Y., Coward, A. C., and Anderson, T. R.: Regional variability of acidification in the Arctic: a sea of contrasts, Biogeosciences, 11, 293–308, doi:10.5194/bg-11-293-2014, 2014.

BGD
12, 5907–5940, 2015

Ricke, K. L., Orr, J. C., Schneider, K., and Caldeira, K.: Risks to coral reefs from ocean carbonate chemistry changes in recent earth system model projections, Environ. Res. Lett., 8, 034003, doi:10.1088/1748-9326/8/3/034003, 2013.
Riley, J. P. and Tongudai, M.: The major cation/chlorinity ratios in sea water, Chem. Geol., 2, 263–269, doi:10.1016/0009-2541(67)90026-5, 1967.
Sarma, V. V. S. S., Lenton, A., Law, R. M., Metzl, N., Patra, P. K., Doney, S., Lima, I. D., Dlugokencky, E., Ramonet, M., and Valsala, V.: Sea–air CO_2 fluxes in the Indian Ocean between 1990 and 2009, Biogeosciences, 10, 7035–7052, doi:10.5194/bg-10-7035-2013, 2013.
Sarmiento, J. L. and Gruber, N.: Sinks for Anthropogenic Carbon, Phys. Today, 55, 30–36, doi:10.1063/1.1510279 , 2002.
Sarmiento, J. L. and Gruber, N.: Ocean Biogeochemical Dynamics, Princeton University Press, 526 pp., Princeton, 2006.
Sasse, T. P., McNeil, B. I., and Abramowitz, G.: A novel method for diagnosing seasonal to inter-annual surface ocean carbon dynamics from bottle data using neural networks, Biogeosciences, 10, 4319–4340, doi:10.5194/bg-10-4319-2013, 2013a.
Sasse, T. P., McNeil, B. I., and Abramowitz, G.: A new constraint on global air–sea CO_2 fluxes using bottle carbon data, Geophys. Res. Lett., 40, 1594–1599, doi:10.1002/grl.50342, 2013b.
Schuster, U., Watson, A. J., Bates, N. R., Corbiere, A., Gonzalez-Davila, M., Metzl, N., Pierrot, D., and Santana-Casiano, M.: Trends in North Atlantic sea-surface fCO_2 from 1990 to 2006, Deep-Sea Res. Pt. II, 56, 620–629, doi:10.1016/j.dsr2.2008.12.011, 2009.
Séférian, R., Bopp, L., Gehlen, M., Orr, J., Ethé, C., Cadule, P., Aumont, O., Salas y Mélia, D., Voldoire, A., and Madec, G.: Skill assessment of three earth system models with common marine biogeochemistry, Clim. Dynam., 40, 2549–2573, doi:10.1007/s00382-012-1362-8, 2013.
Shaw, E. C., Munday, P. L., and McNeil, B. I.: The role of CO2 variability and exposure time for biological impacts of ocean acidification, Geophys. Res. Lett., 40, 4685–4688, doi:10.1002/grl.50883, 2013.
Steinacher, M., Joos, F., Frölicher, T. L., Plattner, G.-K., and Doney, S. C.: Imminent ocean acidification in the Arctic projected with the NCAR global coupled carbon cycle-climate model, Biogeosciences, 6, 515–533, doi:10.5194/bg-6-515-2009, 2009.
Takahashi, T., Sutherland, S. C., Wanninkhof, R., Sweeney, C., Feely, R. A., Chipman, D. W., Hales, B., Friederich, G., Chavez, F., Sabine, C. L., Watson, A., Bakker, D. C. E., Schus-

BGD
12, 5907–5940, 2015

ter, U., Metzl, N., Yoshikawa-Inoue, H., Ishii, M., Midorikawa, T., Nojiri, Y., Körtzinger, A., Steinhoff, T., Hoppema, M., Olafsson, J., Arnarson, T. S., Tilbrook, B., Johannessen, T., Olsen, A., Bellerby, R. G. J., Wong, C. S., Delille, B., Bates, N. R., and de Baar, H. J. W.: Climatological mean and decadal change in surface ocean pCO_2, and net sea–air CO_2 flux over the global oceans, Deep-Sea Res. Pt. II, 56, 554–577, doi:10.1016/j.dsr2.2008.12.009, 2009.

Takahashi, T., Sutherland, S. C., Chipman, D. W., Goddard, J. G., Ho, C., Newberger, T., Sweeney, C., and Munro, D. R.: Climatological distributions of pH, pCO_2, total CO_2, alkalinity, and $CaCO_3$ saturation in the global surface ocean, and temporal changes at selected locations, Mar. Chem., 164, 95–125, doi:10.1016/j.marchem.2014.06.004, 2014.

Tupper, M., Tan, M. K., Tan, S. L., Radius, M. J., and Abdullah, S.: ReefBase: a global information system on coral reefs, available at: http://www.reefbase.org (last access: 2013), 2011.

Zahariev, K., Christian, J. R., and Denman, K. L.: Preindustrial, historical, and fertilization simulations using a global ocean carbon model with new parameterizations of iron limitation, calcification, and N2 fixation, Prog. Oceanogr., 77, 56–82, doi:10.1016/j.pocean.2008.01.007, 2008.

Zweng, M. M., Reagan, J. R., Antonov, J. I., Locarnini, R. A., Mishonov, A. V., Boyer, T. P., Garcia, H. E., Baranova, O. K., Johnson, D. R., D.Seidov, and Biddle, M. M.: World Ocean Atlas 2013, Volume 2: Salinity, edited by: Levitus, S. and Mishonov, A., NOAA Atlas NESDIS 74, 39 pp., Maryland, 2013.

BGD
12, 5907–5940, 2015

Table 1. Main characteristics of the 6 ESM used in this study.

Model	Ocean Resolution	BGC model	Reference
CanESM2	0.9–1.4°	CMOC	Zahariev et al. (2008)
GFDL-ESM2G	0.3–1°	TOPAZ2	Dunne et al. (2013)
HadGEM2-ES	0.3–1°	Diat-HadOCC	Palmer and Totterdell (2001)
IPSL-CM5A-LR	0.5–2°	PISCES	Aumont and Bopp (2006), Séférian et al. (2013)
IPSL-CM5A-MR	0.5–2°	PISCES	Aumont and Bopp (2006), Séférian et al. (2013)
MPI-ESM-MR	0.4°	HAMOCC5.2	Ilyina et al. (2013)

BGD
12, 5907–5940, 2015

Table 2. Comparison between future aragonite projections under RCP4.5 and 2.6 relative to RCP8.5.

RCP	Month-long onset mean ± SD (RCP8.5)	Atmospheric CO_2 mean ± SD (RCP8.5)	Corr. to RCP8.5	Number of 1° × 1° grid cells
		North Pacific (30 to 65° N)		
4.5	2052 ± 27 (2037 ± 18)	481 ± 54 (491 ± 69)	0.82	576
2.6	2017 ± 20 (2017 ± 15)	398 ± 28 (414 ± 45)	0.84	172
		North Atlantic (30 to 70° N)		
4.5	2058 ± 24 (2043 ± 16)	495 ± 50 (518 ± 70)	0.86	60
2.6	2017 ± 10 (2011 ± 18)	399 ± 26 (395 ± 30)	0.91	10
		Southern Ocean (South of 45° S)		
4.5	2064 ± 19 (2045 ± 9)	505 ± 14 (518 ± 9)	0.75	2695
2.6	2030 ± 14 (2030 ± 9)	427 ± 20 (450 ± 30)	0.67	160

BGD
12, 5907–5940, 2015

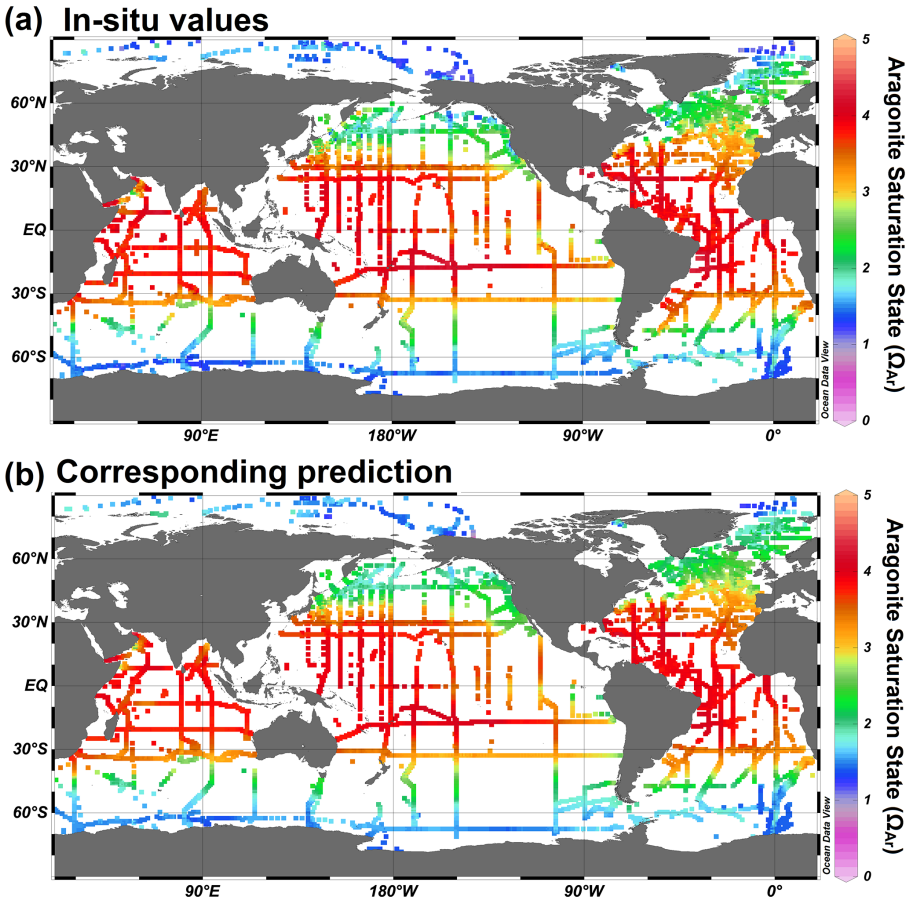

Figure 1. (a) In-situ Ω_{Ar} measurements normalised to the year 2000; **(b)** corresponding $1^\circ \times 1^\circ$ Ω_{Ar} prediction for the same month and for the nominal year for 2000 (see Sect. S1 in the Supplement for our monthly Ω_{Ar} distributions).

BGD
12, 5907–5940, 2015

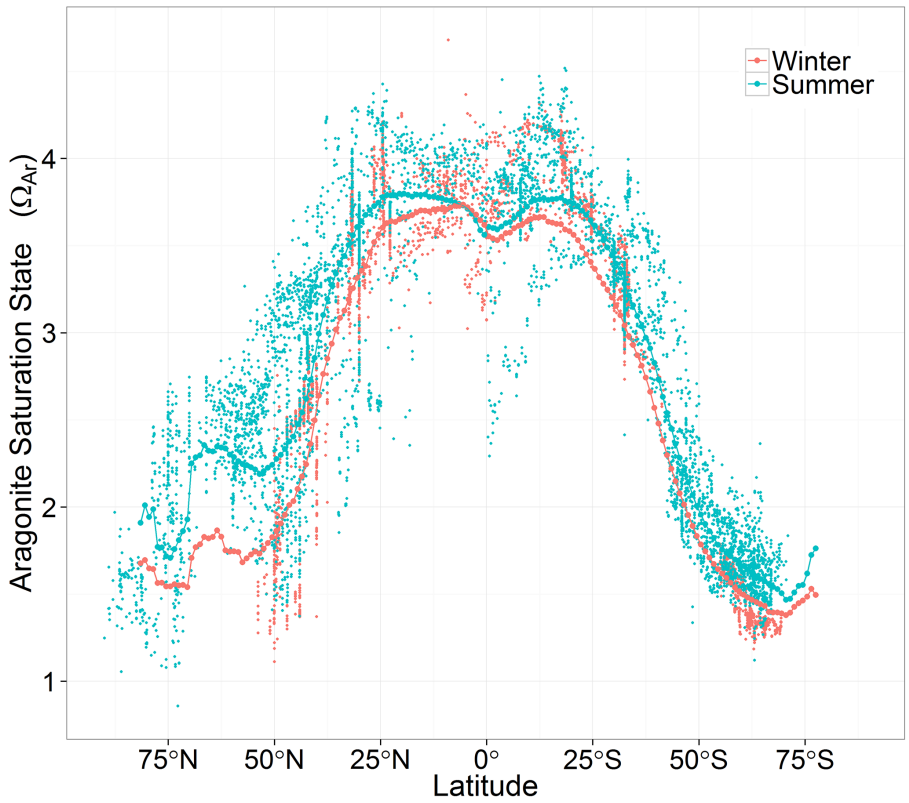

Figure 2. Zonal mean Ω_{Ar} predictions for winter and summer (joined dots). In-situ Ω_{Ar} values normalized to the year 2000. Summer and winter months were defined as June through to August and December through to February for Northern Hemisphere respectively, while Southern Hemisphere differed by 6 months.

BGD
12, 5907–5940, 2015

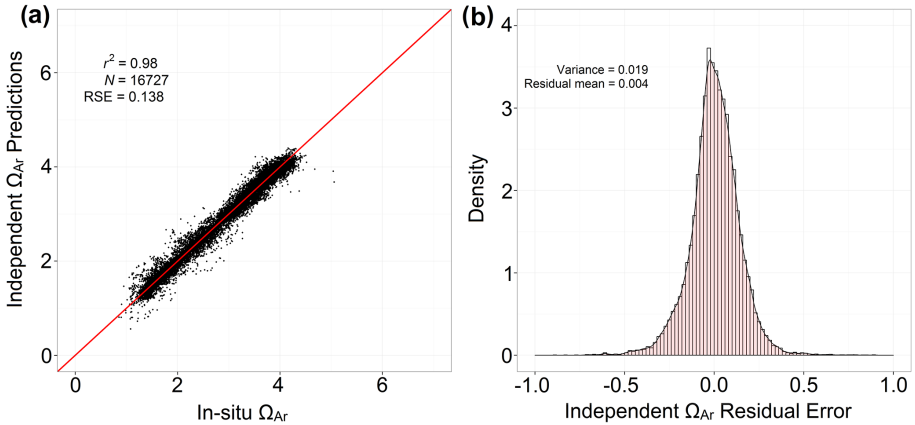

Figure 3. Statistical plots comparing global Ω_{Ar} values calculated via the in-situ network of C_T and A_T measurements, and independently predicted C_T and A_T values via the approach of Sasse et al. (2013b). **(a)** Independent predictions vs. in-situ values, where the red line represents $y = x$ relationship; **(b)** global distribution of the independent residual errors.

BGD
12, 5907–5940, 2015

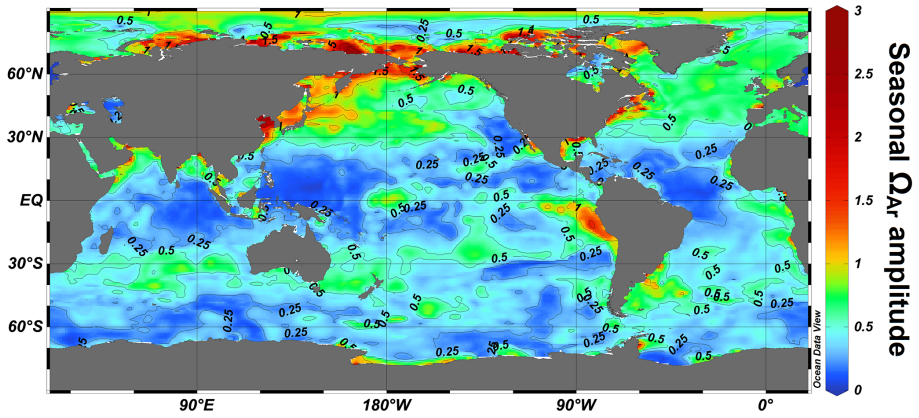

Figure 4. Seasonal Ω_{Ar} amplitudes for the nominal year of 2000. Seasonal amplitudes were calculated as the maximum minus minimum monthly Ω_{Ar} values in each $1^\circ \times 1^\circ$ cell (see Sect. S1 for monthly Ω_{Ar} distributions).

BGD
12, 5907–5940, 2015

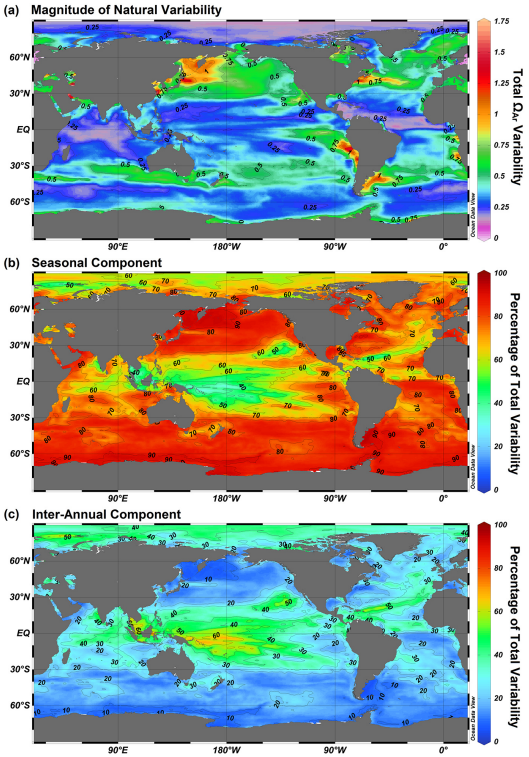

Figure 5. Model-based comparison of seasonal and inter-annual variability for ocean surface Ω_{Ar}. **(a)** Total magnitude of variability as estimated from the ensemble of ESM. Here seasonal variability was calculated as the mean seasonal amplitude between 2006 and 2016, while IAV was calculated via the SD in de-trended annual mean projections between 2006 and 2100; **(b)** relative contribution of seasonal variability to the total variability (in percentage); **(c)** relative contribution of inter-annual variability to the total variability (in percentage).

BGD
12, 5907–5940, 2015

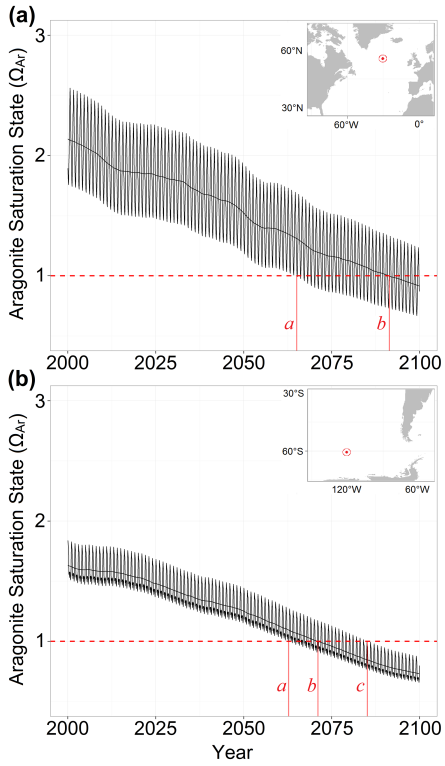

Figure 6. Under RCP8.5 the future aragonite under-saturation states (Ω_{Ar}) at locations in the **(a)** North Atlantic and **(b)** Southern Ocean under the *business-as-usual* (RCP8.5). The influence of seasonal variability accelerates under-saturation conditions by 27 and 8 years relative to annual-mean estimates (black line) in the North Atlantic and Southern Ocean, respectively. The red points *a*, *b*, and *c* denote the time when month-long, annual-mean and permanent under-saturation occurs, respectively.

BGD
12, 5907–5940, 2015

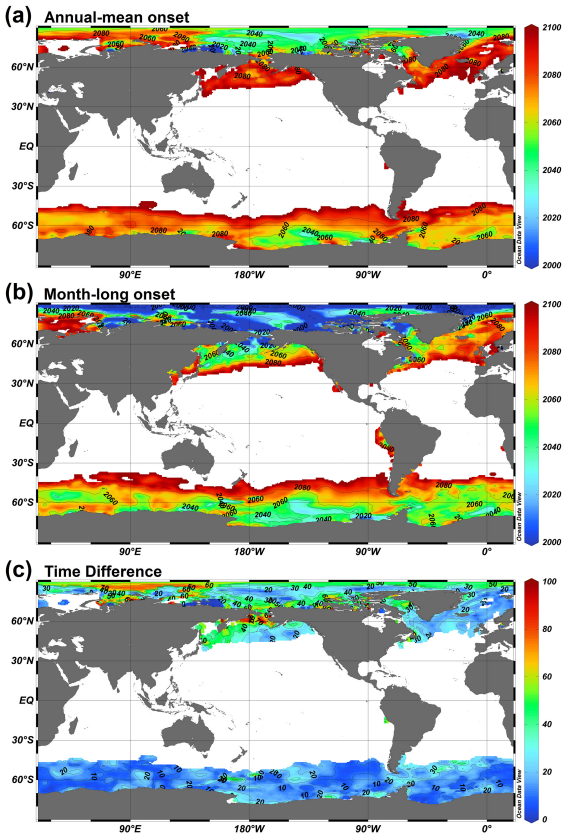

Figure 7. Estimated onset year for aragonite under-saturation within the 21st century under RCP8.5 for **(a)** annual-mean and **(b)** one-month. **(c)** Time difference (years) between annual-mean and month-long estimates.

BGD
12, 5907–5940, 2015

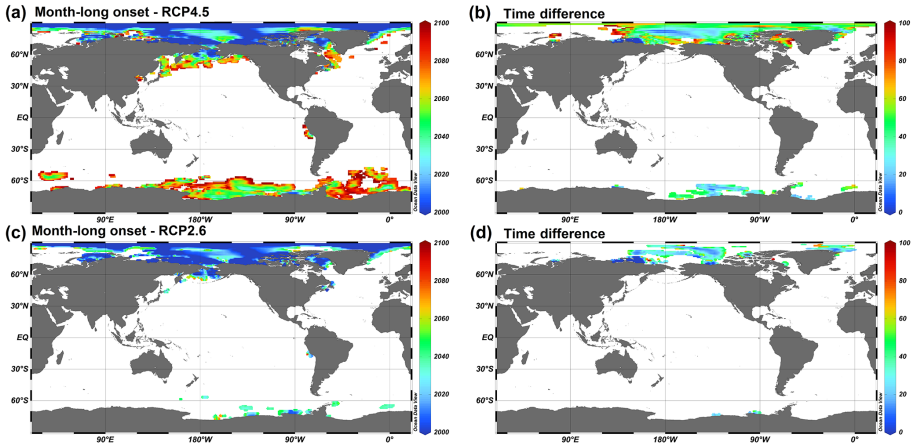

Figure 8. Onset year for month-long ocean surface aragonite under-saturation for **(a)** RCP4.5 and **(c)** RCP2.6. Time difference (years) between month-long and annual-mean surface aragonite under-saturation onset under **(b)** RCP4.5 and **(d)** RCP2.6.

BGD
12, 5907–5940, 2015

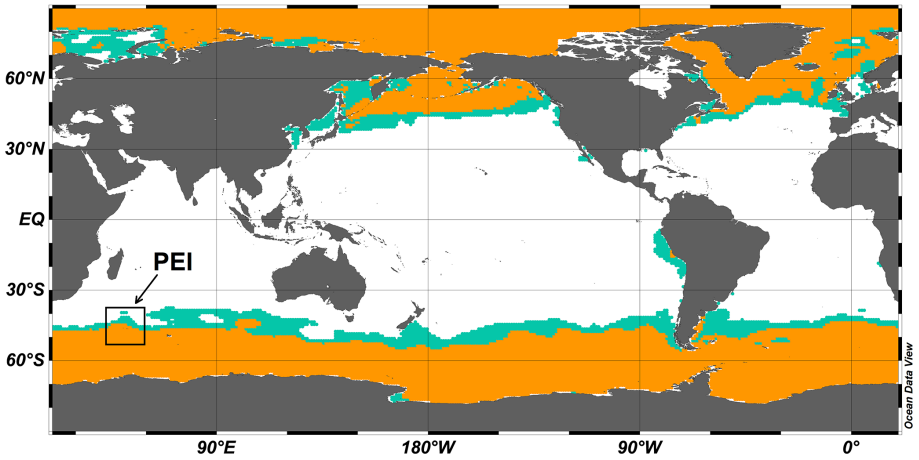

Figure 9. Surface area exposed to at least month-long (blue) and annual-mean (orange) aragonite under-saturation in the year 2100 under RCP8.5. The blue region represents ~ 25×10^6 km^2. The area labelled PEI represents the pteropod study region of Hunt et al. (2008) around the Prince Edward Islands.

BGD
12, 5907–5940, 2015